Supporting information for

Fe-Mediated Nitrogen Fixation with a Metallocene Mediator: Exploring pK_a Effects and Demonstrating Electrocatalysis

Matthew J. Chalkley,[†] Trevor J. Del Castillo,[†] Benjamin D. Matson,[†] and Jonas C. Peters*

[†]M.J.C., T.J.D.C., and B.D.M. contributed equally to this work.

Division of Chemistry and Chemical Engineering, California Institute of Technology, Pasadena, California 91125, United States

Table of Contents:

S1. Experimental Details

S1.1. General Considerations

All manipulations were carried out using standard Schlenk or glovebox techniques under an N_2 atmosphere. Solvents were deoxygenated and dried by thoroughly sparging with N_2 followed by passage through an activated alumina column in a solvent purification system by SG Water, USA LLC. Non-halogenated solvents were tested with sodium benzophenone ketyl in tetrahydrofuran (THF) in order to confirm the absence of oxygen and water. Deuterated solvents were purchased from Cambridge Isotope Laboratories, Inc., degassed, and dried over activated 3-Å molecular sieves prior to use.

Cp^*_2Co,[1] $[P_3^BFe][BAr^F_4]$,[2] $[P_3^BFeN_2][Na(Et_2O)_3]$,[3] $[P_3^BFeN_2][Na(12\text{-crown-4})_2]$,[3] $[H(OEt2)][BAr^F_4]$ ($HBAr^F_4$; BAr^F_4 = tetrakis- (3,5-bis(trifluoromethyl)phenyl)borate)[4], sodium BAr^F_4 ($NaBAr^F_4$)[4], and ^{15}N-diphenylammonium triflate ($[Ph_2{}^{15}NH_2][OTf]$)[5,6] were prepared according to literature procedures. All other reagents were purchased from commercial vendors and used without further purification unless otherwise stated. Diethyl ether (Et_2O) used in the experiments herein was stirred over Na/K (≥ 2 hours) and filtered through celite before use.

S1.2. Gas Chromatography

H_2 was quantified on an Agilent 7890A gas chromatograph (HP-PLOT U, 30 m, 0.32 mm ID; 30 °C isothermal; nitrogen carrier gas) using a thermal conductivity detector. A 10 mL manual injection was used and integration area was converted to percent H_2 composition by use of a calibration obtained from injection of H_2 solutions in N_2 of known concentration.

S1.3. Mössbauer Spectroscopy

Mössbauer spectra were recorded on a spectrometer from SEE Co. (Edina, MN) operating in the constant acceleration mode in a transmission geometry. The sample was kept in an SVT-400 cryostat form Janis (Wilmington, MA). The quoted isomer shifts are relative to the centroid of the spectrum of a metallic foil of α-Fe at room temperature (RT). Solution samples were transferred to a sample cup and freeze-quenched with liquid nitrogen inside of the glovebox and then immersed in liquid N_2 until mounted in the cryostat. Data analysis was performed using version 4 of the program WMOSS (www.wmoss.org) and quadrupole doublets were fit to Lorentzian lineshapes. See discussion below for detailed notes on the fitting procedure.

S1.4. Ammonia Quantification

Reaction mixtures are cooled to 77 K and allowed to freeze. The reaction vessel is then opened to atmosphere and to the frozen solution is slowly added a twofold excess (with respect to acid) solution of a NaO^tBu solution in MeOH (0.25 mM) over 1-2 minutes. This solution is allowed to freeze and a Schlenk tube adapter is added and the headspace of the tube is evacuated. After sealing the tube is then allowed to warm to RT and stirred at RT for at least 10 minutes. An additional Schlenk tube is charged with HCl (3 mL of a 2.0 M solution in Et_2O, 6 mmol) to serve as a collection flask. The volatiles of the reaction mixture are vacuum transferred at RT into this collection flask. After completion of the vacuum transfer, the collection flask is sealed and warmed to RT and stirred vigorously for 10 minutes. Solvent is removed in vacuo, and the remaining residue is dissolved in DMSO-d_6 containing 20 mM 1,3,5-trimethoxybenzene as an

internal standard. The ammonium chloride is quantified by integration relative to the 1,3,5-trimethoxybenzene internal standard.

S1.5. Computational Methods

All stationary point geometries were calculated using DFT-D_3 (Grimmes D_3 dispersion correction[7]) with an TPSS functional,[8] a def2-TZVP[9] basis set on transition metals and a def2-SVP[7] basis set on all other atoms. Calculations were performed, in part, using Xtreme Science and Engineering Discovery Environment (XSEDE) resources.[10] Calculations were performed on the full P_3^BFe scaffold. Geometries were optimized using the NWChem 6.5 package.[11] All single point energy, frequency and solvation energy calculations were performed with the ORCA package.[12] Frequency calculations were used to confirm true minima and to determine gas phase free energy values (G_{gas}). Single point solvation calculations were done using an SMD solvation model[13, 14] with diethyl ether solvent and were used to determine solvated internal energy (E_{soln}). Free energies of solvation were approximated using the difference in gas phase internal energy (E_{gas}) and solvated internal energy ($\Delta G_{solv} \approx E_{soln} - E_{gas}$) and the free energy of a species in solution was then calculated using the gas phase free energy (G_{gas}) and the free energy of solvation ($G_{soln} = G_{gas} + \Delta G_{solv}$).[15,16] All reduction potentials were calculated referenced to $Fc^{+/0}$ and using the standard Nernst relation $\Delta G = -nFE^0$.

S2. Synthetic Details:

S2.1. General Procedure for the Synthesis of the Anilinium Triflates[17,18]

Prior to use the amine was purified (aniline and 2,6-dimethylaniline by distillation and the remaining substituted anilines by sublimation). To a 100 mL round bottom flask in the glovebox was added the desired aniline which was subsequently dissolved in 50 mL of Et_2O (no additional drying with NaK). To this was added dropwise (1 equiv) of HOTf with stirring over five minutes. Immediate precipitation of white solid was observed and the reaction mixture was allowed to stir for thirty minutes. The reaction mixture was then filtered and the resulting white powder was washed with Et_2O (50 mL) and pentane (50 mL). The resulting white microcrystalline material was then dried under vacuum. Yields of greater than 90% of microcrystalline material was obtained in this manner in all cases.

4-methoxyanilinium triflate ([$^{4\text{-OMe}}$PhNH$_3$][OTf]): ^{1}H NMR (DMSO-*d*6, 400 MHz): 7.52 (m, 2 H), 7.28 (m, 2H), 4.30 (br, 3H).

anilinium triflate ([PhNH$_3$][OTf]): ^{1}H NMR (DMSO-*d*6, 400 MHz): 7.50 (m, 2 H), 7.41 (m, 1H), 7.34 (m, 2H).

2,6-dimethylanilinium triflate ([$^{2,6\text{-Me}}$PhNH$_3$][OTf]): ^{1}H NMR (DMSO-*d*6, 400 MHz): 7.14 (m, 3H), 2.32 (br, 6H).

2-chloroanilinium triflate ([$^{2\text{-Cl}}$PhNH$_3$][OTf]): ^{1}H NMR (DMSO-*d*6, 400 MHz): 7.32 (m, 1H), 7.15 (m, 1H), 7.02 (m, 1H), 6.82 (m, 1H).

2,5-chloroanilinium triflate ([$^{2,5\text{-Cl}}$PhNH$_3$][OTf]): ^{1}H NMR (DMSO-*d*6, 400 MHz): 7.19 (apparent d, 1H, ^{3}J(H-H) = 8.5 Hz), 6.83 (apparent dd, 1H, ^{3}J(H-H) = 2.5 Hz, 0.9 Hz), 6.56 (m, 1H).

2,6-chloroanilinium triflate ([$^{2,6\text{-Cl}}$PhNH$_3$][OTf]): ^{1}H NMR (DMSO-*d*6, 400 MHz): 7.22 (d, 2H, ^{3}J(H-H) = 8.0 Hz), 6.57 (t, 1H, ^{3}J(H-H) = 8.0 Hz).

2,4,6-chloroanilinium triflate ([$^{2,4,6\text{-Cl}}$PhNH$_3$][OTf]): ^{1}H NMR (DMSO-*d*6, 400 MHz): 7.37 (s, 2H).

S2.2. Preparation of decamethylcobaltocenium tetrakis(3,5-bis(trifluoromethyl)phenyl)borate), [Cp*$_2$Co][BAr$^F_4$]

A RT solution of HBAr$^F_4$ (96.1 mg, 0.095 mmol) in Et$_2$O (6 mL) is added dropwise to a stirred, RT solution of Cp*$_2$Co (32.9 mg, 0.1 mmol) in Et$_2$O (6 mL). This mixture is allowed to stir 30 min and then reduced to dryness in vacuo. The resulting solid residue is washed with pentane (3 x 2 mL) to yield [Cp*$_2$Co][BAr$^F_4$] as a bright yellow solid (104 mg isolated, 92% yield).

^{1}H NMR (THF-*d*8, 300 MHz): δ 7.79 (8H, s, BAr$^F_4$), δ 7.58 (4H, s, BAr$^F_4$), δ 1.75 (30H, s, Cp*$_2$Co).

S3. Ammonia Generation Details

S3.1. Standard NH$_3$ Generation Reaction Procedure

All solvents are stirred with Na/K for ≥ 2 hours and filtered prior to use. In a nitrogen-filled glovebox, the precatalyst (2.3 μmol) was weighed into a vial. The precatalyst was then transferred quantitatively into a long tube with a female 24-40 joint at the top using THF. The THF was then evaporated to provide a thin film of precatalyst at the bottom of tube. The tube is then charged with a stir bar, the acid (108 equiv), and Cp*$_2$Co (41.2 mg, 54 equiv) as solids. The tube is then sealed at RT with a septum that is secured with copper wire (this ensures a known volume of N_2 in the reaction vessel, which is important for H_2 detection). The tube is then chilled to 77 K and allowed to equilibrate for 10 minutes. To the chilled tube is added 1 mL of Et$_2$O. The temperature of the system is allowed to equilibrate for 5 minutes. This tube is passed out of the box into a liquid N_2 bath and transported to a fume hood. The tube is then transferred to a dry ice/acetone bath where it thaws and is allowed to stir at −78 °C for four hours. At this point the headspace of the tube is sampled with a 10 mL sealable gas syringe which is used to analyze for H_2 by GC. The tube is then allowed to warm to RT with stirring and then stirred at RT for a further ten minutes. At this point the previously described procedure for quantifying ammonia was employed. To ensure reproducibility, all experiments were conducted in 395 mL tubes (51 mm OD) using 25 mm stir bars and stirring was conducted at ~ 650 rpm.

Table S1: NMR quantification results for standard NH_3 generation experiments with [P$_3^B$Fe][BAr$^F_4$]

Entry	Acid	Integration Relative to Internal Standard	% Yield NH_3 (error)	% Yield H_2 (error)
1	[$^{4\text{-OMe}}$PhNH$_3$][OTf]	0.01, 0.02	0.2 ± 0.1	89.1 ± 0.2
2	[PhNH$_3$][OTf]	3.42, 3.33	40.4 ± 0.5	48.6 ± 0.7

3	[$^{2,6\text{-Me}}$PhNH$_3$][OTf]	4.30, 3.63	47.5 ± 4.0	37.8 ± 0.2
4	[$^{2\text{-Cl}}$PhNH$_3$][OTf]	4.98, 4.92	59.3 ± 0.4	26.1 ± 1.9
5	[$^{2,5\text{-Cl}}$PhNH$_3$][OTf]	6.78, 6.15	77.5 ± 3.8	10.5 ± 1.1
6	[$^{2,6\text{-Cl}}$PhNH$_3$][OTf]	6.81, 6.00	76.7 ± 4.9	12.6 ± 2.5
7	[$^{2,6\text{-Cl}}$PhNH$_3$][OTf]*	6.60, 5.81	74.4 ± 4.7	14.2 ± 3.4
8	[$^{2,6\text{-Cl}}$PhNH$_3$][BAr$^F{}_4$]	4.12, 3.0	42.7 ± 6.7	18.8 ± 0.8
9	[$^{2,4,6\text{-Cl}}$PhNH$_3$][OTf]	5.73, 6.10	70.9 ± 2.2	12.0 ± 0.8
10	pentachloroanilinium triflate ([$^{\text{per-Cl}}$PhNH$_3$][OTf])	1.62, 1.70	19.9 ± 0.5	63.5 ± 1.1

*Run performed with [P$_3{}^B$FeN$_2$][Na(Et$_2$O)$_3$] as the precatalyst.

S4. H_2 Monitoring Details

S4.1. Standard Background Generation Reaction Procedure

All solvents are stirred with Na/K for ≥ 2 hours and filtered prior to use. In a nitrogen-filled glovebox, a long tube with a female 24-40 joint is charged with a stir bar, the acid (108 equiv) and Cp*$_2$Co (41.2 mg, 54 equiv). The tube is then sealed at RT with a septum that is secured with copper wire. The tube is then chilled to 77 K and allowed to equilibrate for 10 minutes. To the chilled tube is added 1 mL of Et$_2$O. The temperature of the system is allowed to equilibrate for 5 minutes. This tube is passed out of the box into a liquid N_2 bath and transported to a fume hood. The tube is then transferred to a dry ice/acetone bath where it thaws and is allowed to stir at −78 °C for four hours. At this point the headspace of the tube is sampled with a 10 mL sealable gas syringe which is used to analyze for H_2.

Table S2: Data for Background H_2 Quantification Experiments

Acid	GC Integration for H_2	% Yield H_2
[$^{4\text{-OMe}}$PhNH$_3$][OTf]	49.8	31.5
[PhNH$_3$][OTf]	24.0	15.2
[$^{2,6\text{-Me}}$PhNH$_3$][OTf]	8.2	5.2
[$^{2\text{-Cl}}$PhNH$_3$][OTf]	47.2	29.9
[$^{2,5\text{-Cl}}$PhNH$_3$][OTf]	37.1	23.5
[$^{2,6\text{-Cl}}$PhNH$_3$][OTf]	77.8	49.2
[$^{2,4,6\text{-Cl}}$PhNH$_3$][OTf]	34.8	22.0

[per-Cl$PhNH_3$][OTf]	98.3	62.3

S4.2. H_2 Evolution Kinetics

All solvents are stirred with Na/K for ≥ 2 hours and filtered prior to use. For the catalyzed run, the precatalyst was then transferred quantitatively into a Schlenk tube using THF. The THF was then evaporated to provide a thin film of precatalyst at the bottom of the long tube with a female 24-40 joint. The tube is then charged with a stir bar and the [2,6-Cl$PhNH_3$][OTf] (77.9 mg, 108 equiv) and Cp*$_2$Co (41.2 mg, 54 equiv) are added as solids. The tube is then sealed at RT with a septum that is secured with copper wire. The tube is then chilled to 77 K and allowed to equilibrate for 10 minutes. To the chilled tube is added 1 mL of Et_2O. The temperature of the system is allowed to equilibrate for 5 minutes. This tube is passed out of the box into a liquid N_2 bath and transported to a fume hood. The tube is then transferred to a dry ice/acetone bath where it thaws and is allowed to stir at −78 °C. As soon as the stir bar is freed from the frozen solution and stirring begins the timing is started. At the time points noted below the headspace was sampled for H_2 with a 10 mL sealable gas syringe.

Table S3: Time points for catalyzed H_2 evolution from 2,6-dichloroanlinium triflate and Cp*$_2$Co

Time (min)	GC Integration for H_2	% Yield H_2 (error)
5	3.8, 6.4	3.3 ± 0.9
15	11.6, 16.9	9.3 ± 1.8
25	14.7, 26.2	13.4 ± 3.8
35	22.5, 20.8	13.9 ± 0.5

Table S4. Time points for uncatalyzed H_2 evolution from 2,6-dichloroanlinium triflate and Cp*$_2$Co

Time (min)	GC Integration for H_2	% Yield H_2 (error)
5	3.3, 2.9	2.0 ± 0.1
15	7.0, 6.2	4.3 ± 0.3
25	8.8, 11.1	6.3 ± 0.8
65	20.7, 27.0	14.5 ± 1.7

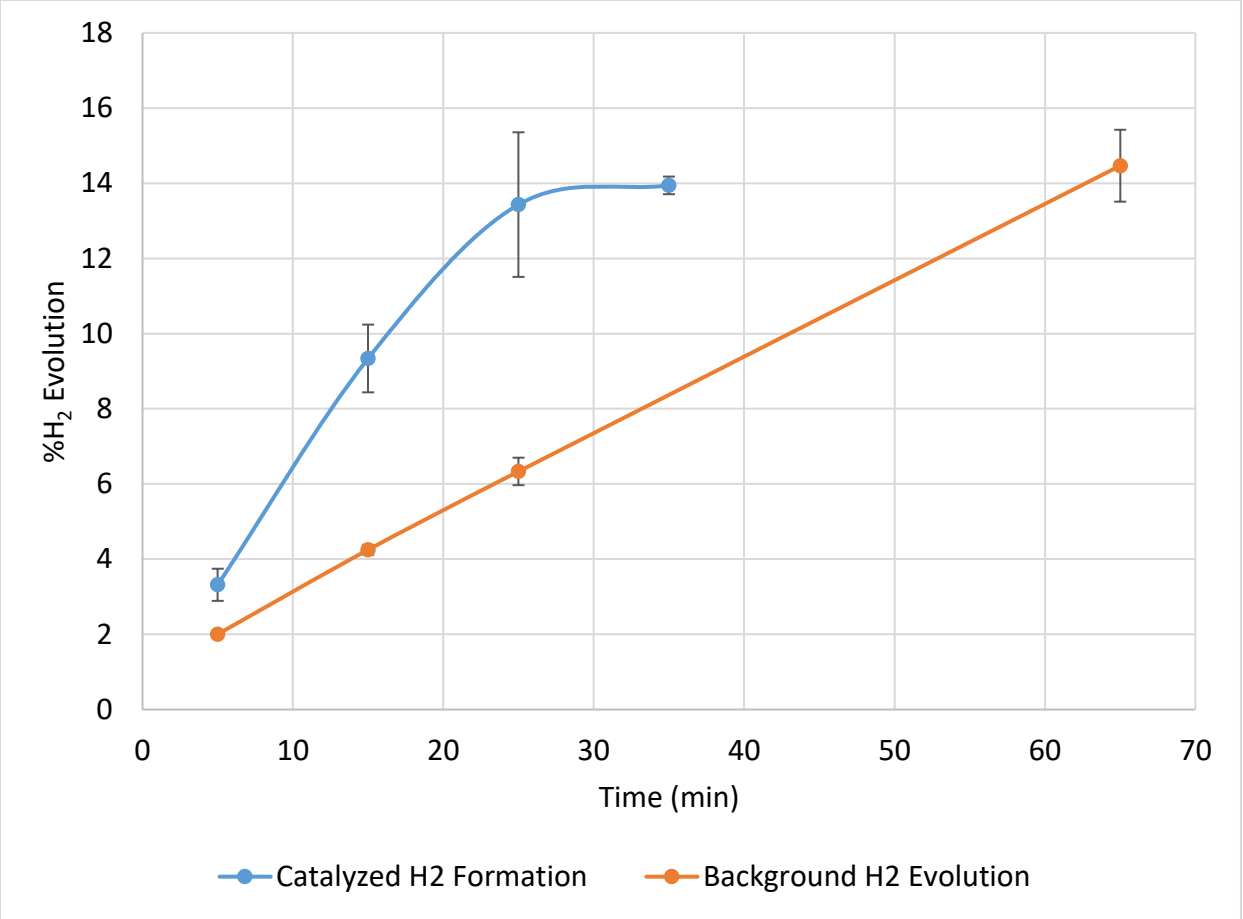

Figure S1: Comparison of catalyzed and uncatalyzed H_2 evolution from 2,6-dichloroanlinium triflate and Cp*$_2$Co at early time points.

S5. Mössbauer Spectroscopy

S5.1. General Procedure for Freeze-Quench Mössbauer Spectroscopy

All solvents are stirred with Na/K for ≥ 2 hours and filtered prior to use. In a nitrogen-filled glovebox, the desired ^{57}Fe species (0.0023 mmol) is quantitatively transferred using THF to a vial and then evaporated to yield a thin film. That vial is charged with a small stir bar and the other reagents as solids. The vial is then chilled to 77 K in a liquid nitrogen bath and allowed to equilibrate for five minutes. To the chilled tube is added 1 mL of Et_2O and this allowed to equilibrate for another five minutes. The vial is then transferred to a cold well that has been pre-cooled for at least fifteen minutes to −78 °C with a dry ice/acetone bath. When the stir bar is freed from the frozen solvent and begins to stir the time is started. At the time noted the stirring is stopped and using a prechilled pipette the reaction mixture is transferred in one portion to a pre-chilled Mössbauer cup sitting in a vial. The vial is then placed in a liquid nitrogen bath causing the reaction mixture to freeze in approximately twenty seconds. The Mössbauer cup is then submerged in the liquid nitrogen and then removed from the glovebox and standard procedure is used to mount the sample on the Mössbauer spectrometer.

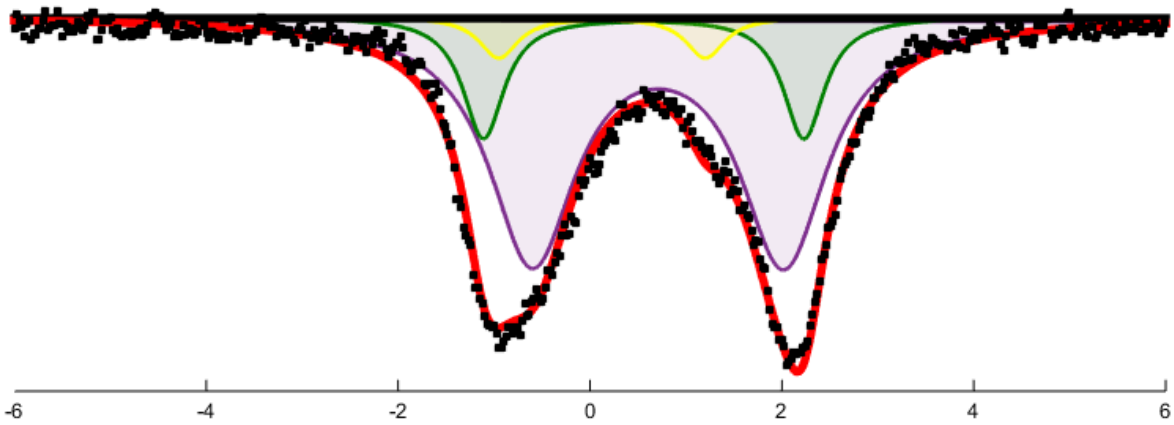

Figure S2. Mössbauer spectrum collected from a reaction freeze quenched after stirring for 5 minutes at −78 °C in 1 mL of Et_2O between $[P_3^B(^{57}Fe)N_2][Na(Et_2O)_3]$ and excess 2,6-$[^{2,6\text{-}Cl}PhNH_3][OTf]$ (50 equiv). Raw data shown as black points, simulation as a solid red line, with components in green, purple, and yellow (see Table S3 for parameters). The spectrum was collected at 80 K with a parallel applied magnetic field of 50 mT in Et_2O.

Fitting details for Figure S2: Three quadrupole doublets were found to be necessary to obtain an adequate simulation. Although a variety of parameters could potentially simulate the relatively broad absorptions observed here, previous reactivity of $P_3^BFeN_2^-$ with acid[19] suggested that $P_3^BFeN_2$ and $P_3^BFe^+$ were likely products. Satisfyingly if the known isomer shift and quadrupole splitting for one of those species was fixed during the fitting process and the other components were allowed to refine freely the other major component was found to be the complementary species.[19] The third species was always unchanged in these simulations and represents an unknown species. Its presence in the fit is demanded by the inflection point on the more negative side of the right-hand absorbance. Modeling this feature also helps to capture the asymmetry of the left-hand absorbance while using the symmetric line-shapes we expect for $P_3^BFeN_2$ (green) and $P_3^BFe^+$ (purple). The broad linewidths for $P_3^BFe^+$ have been observed previously and may be explained by the existence of unbound and bound varieties of the species with the reaction mixture providing potential ligands such as OTf^-, $^{2,6\text{-}Cl}PhNH_2$, and N_2.

Table S5: Simulation parameters for Mossbauer spectrum in Figure S2.

Component	δ (mm s^{-1})	ΔE_Q (mm s^{-1})	Linewidths, Γ_L/Γ_R (mm s^{-1})	Relative area
A (green)	0.58 ± 0.02	3.28 ± 0.07	0.52/0.52	0.26
B (purple)	0.76 ± 0.02	2.57 ± 0.05	1.10/1.10	0.63
C (yellow)	0.13 ± 0.02	2.24 ± 0.04	0.50/0.50	0.11

S6. EPR Spectroscopy

S6.1 General Procedure for EPR Spectroscopy

All solvents are stirred with Na/K for ≥ 2 hours and filtered prior to use. In a nitrogen-filled glovebox, the desired Fe species (0.0023 mmol) is quantitatively transferred using THF to a vial and then evaporated to yield a thin film. That vial is charged with a small stir bar and the acid (0.116 mmol, 50 equiv) as solids ([$^{2,6\text{-Cl}}$PhNH$_3$][OTf] or [$^{2,6\text{-Cl}}$PhNH$_3$][BAr$^F{}_4$]). The vial is then chilled to 77 K in a liquid nitrogen bath and allowed to equilibrate for five minutes. To the chilled tube is added 1 mL of Et_2O (for HOTf 50 equiv have been dissolved in this 1 mL of Et_2O at RT) and this allowed to equilibrate for another five minutes. The vial is then transferred to a cold well that has been pre-cooled for at least fifteen minutes to −78 °C with a dry ice/acetone bath. When the stir bar is freed from the frozen solvent and begins to stir the time is started. The reaction mixture is stirred for five minutes and then stirring is stopped. Using a pre-chilled pipette approximately 0.5 mL of the reaction mixture is rapidly transferred to a pre-chilled X-band EPR tube. The X-band EPR tube is then placed in a liquid nitrogen bath causing the reaction mixture to freeze in approximately twenty seconds. The EPR tube is then sealed and removed from the glovebox in liquid nitrogen.

S6.2 Comment on Stoichiometric Reactivity

In our attempt to model the catalytic reaction mixture we were interested in the reactivity of $P_3{}^BFeN_2^-$ (observed previously both from mixing [$P_3{}^B$Fe][BAr$^F{}_4$] with excess Cp*$_2$Co and under the catalytic reaction conditions) with acid. In order to achieve this we wanted to prepare independently known $P_3{}^BFeN_2^-$ species to model the proposed catalytic intermediate [$P_3{}^B$FeN$_2$][Cp*$_2$Co]. We chose [$P_3{}^B$FeN$_2$][Na(Et$_2$O)$_3$] because we believed that its solubility in Et_2O likely modeled that of [$P_3{}^B$FeN$_2$][Cp*$_2$Co].

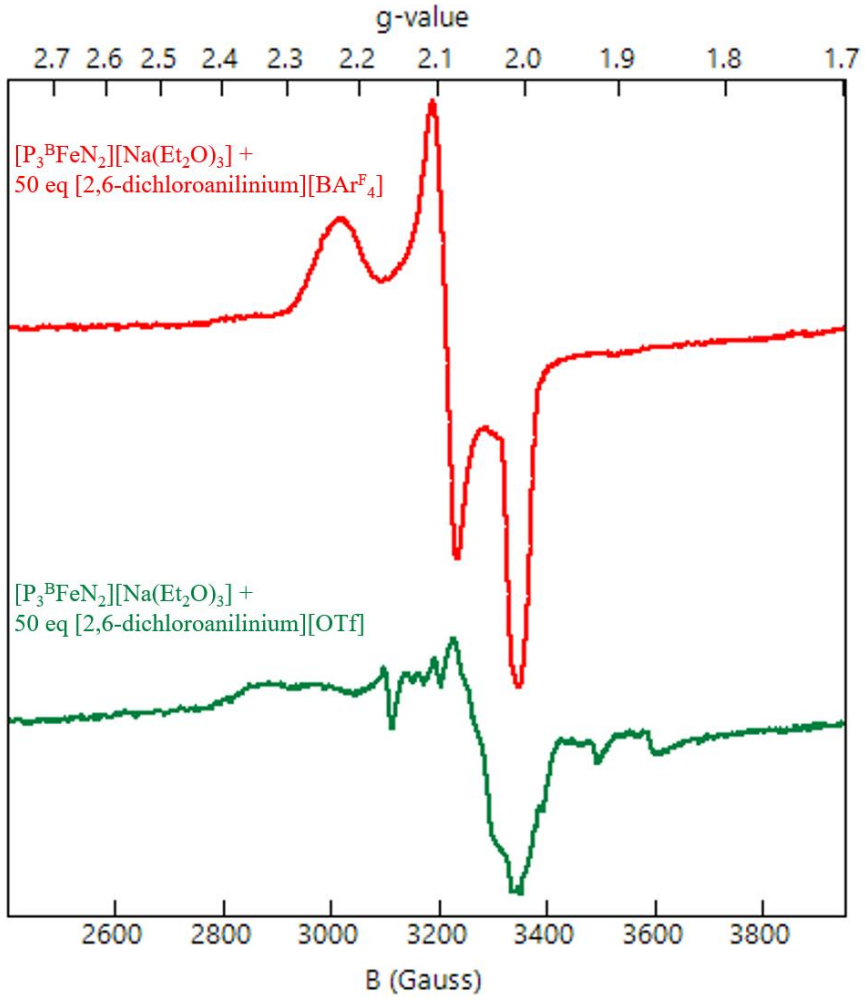

Figure S3: The continuous wave, X-band EPR at 77K in Et_2O of reaction mixtures freeze-quenched after five minutes. In red is the reaction of $[P_3^BFeN_2][Na(Et_2O)_3]$ with 50 equiv of $[^{2,6\text{-}Cl}PhNH_3][BAr^F_4]$ clearly demonstrating the formation of $[P_3^BFeNNH_2][BAr^F_4]$. In green is reaction of $[P_3^BFeN_2][Na(Et_2O)_3]$ with 50 equiv of $[^{2,6\text{-}Cl}PhNH_3][OTf]$ in which the small residual species is neither the starting material ($[P_3^BFeN_2][Na(Et_2O)_3]$) or the desired product ($[P_3^BFeNNH_2][OTf]$). Although we do not know the chemical identity of this species we note that it is very similar to the EPR observed in the reaction of $[P_3^BFeN_2][Na(12\text{-crown-}4)_2]$ with 1 equiv of $HBAr^F_4$.[19] We hypothesize therefore that it may represent a Fe–H side product.

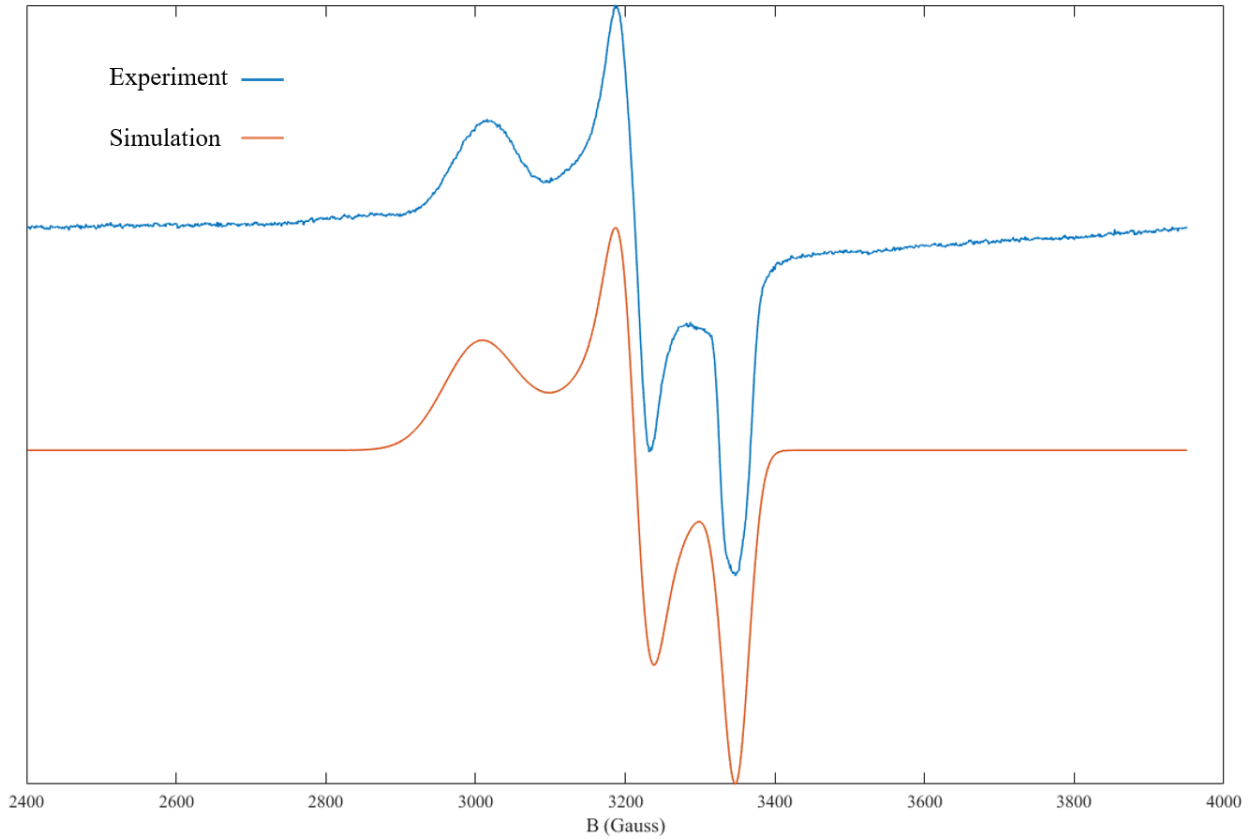

Figure S4: In blue is the continuous wave, X-band EPR spectrum at 77K of a reaction mixture of 50 equiv $[^{2,6\text{-Cl}}PhNH_3][BAr^F{}_4]$ with $[P_3{}^BFeN_2][Na(12\text{-crown-4})_2]$ quenched with liquid nitrogen after 5 minutes. In orange is the simulation of this spectrum (fitting details below)

Fitting details for Figure S4: The parameters used to fit the spectrum were obtained using the esfit application in the easyspin program.[20] The fitting program obtains the best fit by minimizing the root mean square deviation from the data.

The data was fit with the following parameters: $g_1 = 2.23899$, $g_2 = 2.09189$, $g_3 = 2.00664$, and a line broadening of 323.8530, 71.2309, and 38.7902 MHz respectively. These parameters represent only a very small perturbation from those used previously to model $[P_3{}^BFeNNH_2][BAr^F{}_4]$: $g_1 = 2.222$, $g_2 = 2.091$, $g_3 = 2.006$ and a line broadening of 256, 113, and 41 MHz respectively.[19] The slightly broader spectrum observed here precludes resolution of the small phosphorus coupling on g_3. We believe that this broadening arises from either the use of a non-glassing solvent (Et_2O vs 2-MeTHF) or via small differences in hydrogen-bonding that arise from the presence of 2,6-dichloroaniline.

S7. Acid Quench of $P_3{}^BFeN_2^-$

S7.1 Standard Acid Quench Procedure

All solvents are stirred with Na/K for ≥ 2 hours and filtered prior to use. In a nitrogen-filled glovebox, the desired Fe species (2.3 μmol) was weighed into a vial. The Fe species was then transferred quantitatively into a Schlenk tube using THF. The THF was then evaporated to

provide a thin film of Fe species at the bottom of the Schlenk tube. The tube is then charged with a stir bar and acid (0.116 mmol, 50 equiv) as solids 9[$^{2,6\text{-Cl}}$PhNH$_3$][OTf] or [$^{2,6\text{-Cl}}$PhNH$_3$][BAr$^F_4$]) is added as a solid. The tube is then sealed at RT with a septum and a Konte's valve that is left partially open. The tube is then chilled to 77 K and allowed to equilibrate for 10 minutes. To the chilled tube is added 1 mL of Et_2O through the septum. The temperature of the system is allowed to equilibrate for 5 minutes and then the Konte's valve is sealed. This tube is passed out of the box into a liquid N_2 bath and transported to a fume hood. The tube is then transferred to a dry ice/acetone bath where it thaws and is allowed to stir at −78 °C for three hours. At the end of the reaction the Konte's valve is opened and the reaction headspace is allowed to equilibrate. At this point the headspace of the tube is sampled with a 10 mL sealable gas syringe which is used to analyze for H_2. The tube is then allowed to warm to RT with stirring and then stirred at RT for a further ten minutes. At this point the previously described procedure for quantifying ammonia was employed.

Table S6. Comparative NH_3 and H_2 Yields for [$^{2,6\text{-Cl}}$PhNH$_3$][OTf] and [$^{2,6\text{-Cl}}$PhNH$_3$][BAr$^F_4$]

Acid	Yield of NH_3 (equiv)	% Yield H_2
[$^{2,6\text{-Cl}}$PhNH$_3$][OTf]	0.0 ± 0.0	43.7 ± 4.6
[$^{2,6\text{-Cl}}$PhNH$_3$][BAr$^F_4$]	0.20 ± 0.03	37.8 ± 7.6

S8. Solubility Measurement

S8.1. Procedure for Measuring Solubility of Cp*$_2$Co:

All solvents are stirred with Na/K for ≥ 2 hours and filtered prior to use. In a nitrogen-filled glovebox, a Schlenk tube is charged with a stir bar and the Cp*$_2$Co (41.2 mg, 0.125 mmol) is added to the tube. The tube is then chilled to 77 K in a liquid nitrogen bath and allowed to equilibrate for 5 minutes. To the chilled tube is added 1 mL of Et_2O. The temperature of the system is allowed to equilibrate for 5 minutes and then the Schlenk tube is transferred to the cold well which has been prechilled to −78 °C for fifteen minutes. After five minutes of stirring at ~ 620 rpm, the stirring is stopped. With a prechilled pipette the entirety of the reaction mixture is transferred to a similarly prechilled celite pad for filtration. Filtration yielded a pale green solution that was then warmed to RT and the solvent was removed under reduced pressure. The vial was then extracted with a 20 mM solution of 1,3,5-trimethoxybenzene in C_6D_6. The NMR was then measured and the Cp*$_2$Co signal was integrated relative to the 1,3,5-trimethoxybenzene standard. The accuracy of this integration procedure was confirmed by performing this procedure on a sample of Cp*$_2$Co that had simply been weighed into a vial. Repetition of this experiment resulted in Cp*$_2$Co concentrations between 5-6 mM.

S8.2. Procedure for Measuring Solubility of [$^{2,6\text{-Cl}}$PhNH$_3$][OTf]:

All solvents are stirred with Na/K for ≥ 2 hours and filtered prior to use. In a nitrogen-filled glovebox, a Schlenk tube is charged with a stir bar and the [$^{2,6\text{-Cl}}$PhNH$_3$][OTf] (77.9 mg, 0.250 mmol) is added to the tube. The tube is then chilled to 77 K in a liquid nitrogen bath and allowed to equilibrate for 5 minutes. To the chilled tube is added 1 mL of Et_2O. The temperature of the system is allowed to equilibrate for 5 minutes and then the Schlenk tube is transferred to the cold

well which has been prechilled to −78 °C for fifteen minutes. After five minutes of stirring at ~ 620 rpm, the stirring is stopped. With a prechilled pipette the entirety of the reaction mixture is transferred to a similarly prechilled celite pad for filtration. Filtration yielded a colorless solution that was then warmed to RT and the solvent was removed under reduced pressure. The vial was then extracted with a 20 mM solution of 1,3,5-trimethoxybenzene in THF-d_8. The NMR was then measured and the two signals for [$^{2,6\text{-Cl}}$PhNH$_3$][OTf] were integrated relative to the 1,3,5-trimethoxybenzene standard. The result was a [$^{2,6\text{-Cl}}$PhNH$_3$][OTf] concentration of 0.4 mM.

S9. Controlled Potential Electrolysis (CPE) and Cyclic Voltammetry (CV) Details

S9.1. General considerations:

All manipulations are carried out in an N_2-filled glove box. For CPE experiments a sealable H-cell consisting of two compartments separated by a fine porosity sintered glass frit is cooled to −35 °C in a cold well and charged with 4 mL (working chamber) and 4 mL (auxiliary chamber) of 0.1 M NaBAr$^F_4$ solution in Et_2O, the solutions are also cooled to −35 °C and the solution for the working chamber may contain additional chemical components as described below. The working chamber is outfitted with a glassy carbon working electrode, rectangular prismatic in shape with dimensions of 10 mm × 2 mm and submerged in the working chamber solution to a depth of ~ 10 mm. The working chamber is also equipped with a Ag/AgPF$_6$ in 0.1 M NaBAr$^F_4$ Et_2O reference electrode isolated by a CoralPor™ frit (obtained from BASi) and referenced externally to $Fc^{+/0}$. The auxiliary chamber is outfitted with a solid sodium auxiliary electrode (~ 5 mm × ~ 1 mm rectangular prism, submerged to ~ 5 mm). The cell is sealed before electrolysis. The cell is connected to a CH Instruments 600B electrochemical analyzer and controlled potential bulk electrolysis experiments were performed at −35 °C with stirring, cold well external bath temperature maintained by a SP Scientific FTS Systems FC100 immersion cooler.

CV experiments are conducted in a single compartment cell cooled to −35 °C in a cold well in 0.1 M NaBAr$^F_4$ Et_2O solution, again cold well external bath temperature maintained by a SP Scientific FTS Systems FC100 immersion cooler. The working electrode is a glassy carbon disk, the reference electrode is a Ag/AgPF$_6$ in 0.1 M NaBAr$^F_4$ Et_2O reference electrode isolated by a CoralPor™ frit (obtained from BASi) and referenced externally to $Fc^{+/0}$, the auxiliary electrode is a platinum wire. Measurements conducted with a CH Instruments 600B electrochemical analyzer

S9.2. General methodology for controlled potential electrolysis experiments:

To the working chamber is added 3 mg of [P$_3^B$Fe][BAr$^F_4$] (2 μmol), 100 μmol of acid (e.g. [Ph$_2$NH$_2$][OTf]), 0-23.8 mg of [Cp*$_2$Co][BAr$^F_4$] (0-20 μmol), and a magnetic stir bar. The cell is held at a working potential of −2.1 V vs $Fc^{+/0}$ until the current passed in the cell falls to 1% of the initial current pass or until 21.5 hours have passed. After that time the potential bias is removed, the headspace of the cell is sampled with a sealable gas syringe (10 mL), which is immediately analyzed by GC for the presence of H_2. Then an additional 100 μmol of acid in 2 mL 0.1 M NaBAr$^F_4$ solution in Et_2O is injected through rubber septa into both chambers to sequester NH_3 as [NH_4][OTf]. The cell is allowed to stir at −35 °C for 10 minutes and then warmed to RT. The contents of both chambers are then transferred to a Schlenk tube (cell

washed with additional Et_2O) and this material is analyzed for NH_3 by base digestion, vacuum transfer of volatiles, and NMR integration as described in section S1.4

S9.3. Methodology for controlled potential electrolysis experiments with reloading of substrate:

To the working chamber is added 3 mg of $[P_3^BFe][BAr^F_4]$ (2 μmol), 100 μmol of acid (e.g. $[Ph_2NH_2][OTf]$), 0-23.8 mg of $[Cp^*_2Co][BAr^F_4]$ (0-20 μmol), and a magnetic stir bar. The cell is held at a working potential of −2.1 V vs $Fc^{+/0}$ until the current passed in the cell falls to 1% of the initial current pass or until 21.5 hours have passed. After that time the potential bias is removed. An additional 100 μmol of acid in 2 mL 0.1 M $NaBAr^F_4$ solution in Et_2O is then added to the working chamber of the cell via injection through a rubber septum. The cell is then held at a working potential of −2.1 V vs $Fc^{+/0}$ until the current passed in the cell falls to 1% of the initial current pass or until 21.5 hours have passed. After that time the potential bias is removed, the headspace of the cell is sampled with a sealable gas syringe (10 mL), which is immediately analyzed by GC for the presence of H_2. Then an additional 100 μmol of acid in 2 mL 0.1 M $NaBAr^F_4$ solution in Et_2O is injected through rubber septa into both chambers of the cell to sequester NH_3 as $[NH_4][OTf]$. The cell is allowed to stir at −35 °C for 10 minutes and then warmed to RT. The contents of both chambers are then transferred to a Schlenk tube (cell washed with additional Et_2O) and this material is analyzed for NH_3 by base digestion, vacuum transfer of volatiles, and NMR integration as described in section S1.4

Table S7. Controlled Potential Electrolysis Data.

Entry	Acid	Equiv $[Cp^*_2Co][BAr^F_4]$	Time (h)	Charge Passed (C)	Yield of NH_3 (equiv per Fe)	FE NH_3 (%)	FE H_2[a] (%)
1	$[Ph_2NH_2][OTf]$	0	42	7.5	2.3	18	80
2	$[Ph_2NH_2][OTf]$	0	63	6.2	2.8	26	25
3	$[Ph_2NH_2][OTf]$	0	43	5.4	2.6	28	53
Avg					2.6 ± 0.3	24 ± 5	
4[b]	$[Ph_2NH_2][OTf]$	0	43	7.5	2.2	17	67
5[b]	$[Ph_2NH_2][OTf]$	0	43	9.0	3.0	19	22
Avg					2.6 ± 0.6	18 ± 1	
6	$[Ph_2NH_2][OTf]$	1	17	8.1	4.4	31	56
7	$[Ph_2NH_2][OTf]$	1	22	8.3	3.5	24	47
Avg					4.0 ± 0.6	28 ± 5	

8	$[Ph_2NH_2][OTf]$	5	17	8.5	3.9	26	61
9	$[Ph_2NH_2][OTf]$	5	21	9.1	3.5	22	57
10	$[Ph_2NH_2][OTf]$	5	22	9.5	4.6	28	27
Avg					4.0 ± 0.6	25 ± 3	
11	$[Ph_2NH_2][OTf]$	10	21	9.4	3.0	19	64
12	$[Ph_2NH_2][OTf]$	10	10	10.2	5.1	29	47
Avg					4 ± 1	24 ± 7	
13	$[PhNH_3][OTf]$	5	15	9.0	1.2	8	48
14	$[PhNH_3][OTf]$	5	22	7.8	0.6	4	35
Avg					0.9 ± 0.4	6 ± 3	
15	$[^{2,6\text{-Cl}}PhNH_3][OTf]$	5	17	10.6	2.0	11	44
16	$[^{2,6\text{-Cl}}PhNH_3][OTf]$	5	17	10.7	1.7	9	41
Avg					1.9 ± 0.2	10 ± 1	
17[b]	$[Ph_2NH_2][OTf]$	5	32	17.3	6.1	20	43
18[b]	$[Ph_2NH_2][OTf]$	5	22	18.7	6.7	21	32
19[b]	$[Ph_2NH_2][OTf]$	5	37	13.7	4.7	20	38
20[b]	$[Ph_2NH_2][OTf]$	5	41	15.3	4.8	18	52
21[b]	$[Ph_2NH_2][OTf]$	5	43	17.8	5.4	18	31
Avg					5.5 ± 0.9	19 ± 1	
22A[c]	$[Ph_2NH_2][OTf]$	5	21.5	9.5	4.6	28	27
22B[c]	$[Ph_2NH_2][OTf]$	5	11.5	9.2	0.0	0	88
23[d]	$[Ph_2NH_2][OTf]$	5	16	9.2	0.0	0	75
24[e]	$[Ph_2NH_2][OTf]$	5	43	0.0	0.3	N/A	N/A
25[f]	$[Ph_2NH_2][OTf]$	Chemical runs	21.5	N/A	1.3	7.8 e^-	50 e^-
26[f]	$[Ph_2NH_2][OTf]$	Chemical runs	21.5	N/A	2.3	13.8 e^-	31 e^-

Avg					1.8 ± 0.7	11 ± 4	

[a]Some ports of the cell are sealed with septa and one of these is pierced before the electrolysis begins to pressure equilibrate the cell as it cools to −35 °C, we note therefore that H_2 gas may escape from the cell particular during long experiments, indeed a test of H_2 retention in the cell under equivalent conditions revealed leakage of H_2 (60% recovery), thus the detected % yield of H_2 reported here should be considered a lower limit. [b]These experiments were conducted using the reloading protocol as described above. [c]Electrode rinse test as described in main text. [d]Control experiment with no $[P_3^BFe][BAr^F_4]$ included but including a typical loading of 11.9 mg (10 μmol) of $[Cp^*_2Co][BAr^F_4]$. [e]Control experiment in which the cell with all components, including the sodium auxiliary electrode, was assembled and stirred at −35 °C for 43 hours but neither a potential bias was applied, nor were the working and auxiliary electrodes externally connected. This experiment thus interrogates the ability of the sodium electrode to function as a chemical reductant for N_2RR under the CPE conditions. [f]Chemical catalysis runs at −35 °C in 0.1 M $NaBAr^F_4$ Et_2O solution with 50 equiv (100 μmol) of Cp^*_2Co included as a chemical reductant as well as $[P_3^BFe][BAr^F_4]$ (2 μmol) and 100 μmol of acid ($[Ph_2NH_2][OTf]$).

S9.4 Control experiment for the possibility of NH_3 being generated in a chemical rather than electrochemical process during acidic workup:

As per the general CPE methodologies described in S9.2 and S9.3, after electrolysis additional acid is added to the cell to sequester generated NH_3 as an ammonium salt to facilitate transfer of these materials to a Schlenk tube, ultimately allowing NH_3 quantitation via base digestion and vaccum transfer as described in S1.4. This presents the possibility that electrochemically reduced species formed during electrolysis (e.g., $P_3^BFeN_2^-$ and Cp^*_2Co) could react with this additional acid after the electrolysis was complete to generate NH_3 in a chemical reaction. A control experiment to determine the extent to which this type of reactivity might contribute to the total NH_3 yield observed from the CPE experiments was conducted. The H-cell is assembled via the standard methodology and charged with a typical loading of $[P_3^BFe][BAr^F_4]$ (2 μmol) and $[Cp^*_2Co][BAr^F_4]$ (10 μmol, 5 equiv) but without initial acid (i.e., no $[Ph_2NH_2][OTf]$). Electrolysis is then carried out at −2.1 V vs $Fc^{+/0}$ until the current pass in the cell falls to 1% of the initial current passed (in this case 1.12 C of charge were passed, corresponding to 11.6 μmol of reducing equivalents stored in the system, which approaches the theoretical limit of reducing equivalents that the loading of $[P_3^BFe][BAr^F_4]$ (2 μmol) and $[Cp^*_2Co][BAr^F_4]$ (10 μmol) could store) at this potential. This post electrolysis mixture is then treated with acid and analyzed for NH_3 via the standard methodology. This experiment yielded 0.2 equiv NH_3 (relative to Fe) indicating that chemical N_2RR between electrochemically reduced species during the acidic workup is very minor.

S9.5 Additional CV data:

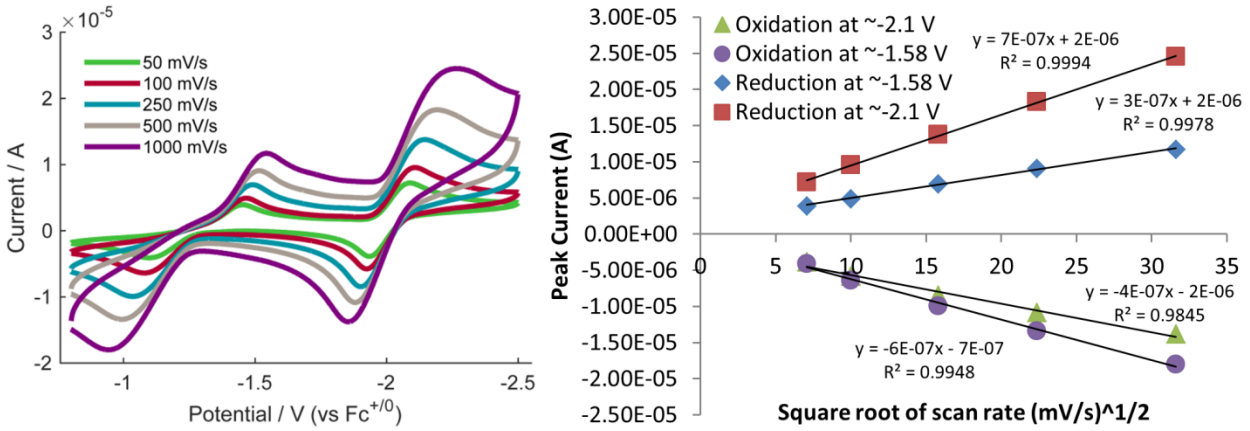

Figure S5. Cyclic voltammograms of 0.5 mM [P_3^BFe][BAr^F_4] at varied scan rates (left) and plot of peak current versus square root of scan rate for each feature (right) showing linear dependence in all cases. All spectra are collected in 0.1 M $NaBAr^F_4$ solution in Et_2O at −35 °C using a glassy carbon working electrode, and externally referenced to the $Fc^{+/0}$ couple.

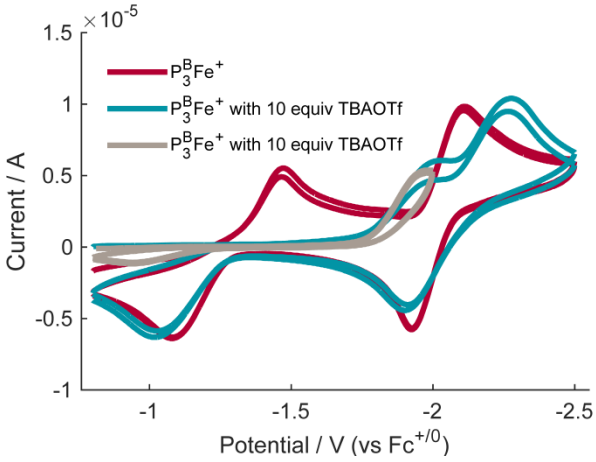

Figure S6. Cyclic voltammograms of 0.5 mM [P_3^BFe][BAr^F_4] (red trace) and [P_3^BFe][BAr^F_4] with 10 equiv of tetrabutylammonium trifluoromethanesulfonate ([TBA][OTf]) (blue and gray traces). The traces with [TBA][OTf] show disappearance of a wave corresponding to the $P_3^BFe^{+/0}$ couple at ~ −1.58 V (present in the red trace). This phenomenon, as in the case with acidic triflate sources as described in the main text, is likely due to triflate binding (to generate P_3^BFeOTf, thereby attenuating the wave associated with the reduction of $P_3^BFe^+$ and $P_3^BFeN_2^+$). If the scan is stopped and reversed at −2.0 (before the $P_3^BFeN_2^{0/-}$ couple) no reversibility is observed, consistent with a chemical step (dissociation of triflate) being coupled with this redox event. We note that in the presence of OTf^- it appears that the second reductive feature is also slightly anodically shifted. We believe this to be due to slow N_2 binding kinetics and thus this wave would represent a convolution of the 0/1− reduction processes for both a vacant and an N_2

bound P_3^BFe. All spectra are collected in 0.1 M $NaBAr^F_4$ solution in Et_2O at −35 °C using a glassy carbon working electrode, and externally referenced to the $Fc^{+/0}$ couple.

S10. Computational Details

S10.1. Calculation of Acid Dissociation Constants

Acid dissociation constants (pK_a and pK_d) were performed were optimized and solvated as discussed in the general methods section. For pK_a values, the ΔG for the exchange of a proton (H^+) between the acid of interest and $^{2,6\text{-Cl}}PhNH_2/^{2,6\text{-Cl}}PhNH_3^+$. For p$K_d$ values, the same approach was used except that the net exchange of a HOTf unit was calculated. In all cases the dissociation constant was reference to the literature value for the pK_a of $^{2,6\text{-Cl}}PhNH_3^+$ in THF.

S10.2. Determination of PT, ET and PCET Kinetics

Kinetic barriers for reported for PT, ET and PCET were performed in one of two ways. Internal consistency between the methods was determined where possible. Values are summarized in Table S8.

Method A. Marcus Theory. Standard Marcus theory expressions[21] were used in method A. Inner sphere reorganization energies for PT or PCET were calculated using the method developed by the group of Hammes-Schiffer (Eq. S1) utilizing the force constants for the reactant (f_j^r) and product (f_j^p) species and the change in equilibrium bond length (Δq_j).[22]

$$\lambda_{is,PT/PCET} = \sum_j \frac{f_j^r f_j^p}{f_j^r + f_j^p} \Delta q_j{}^2 \qquad \text{(Eq. S1)}$$

Outer sphere reorganization energies were calculated using a continuum solvation model for the solvation of a point charge ($\lambda_{os,ET}$)[21] or a dipole ($\lambda_{os,PT}$).[22-24] The $\lambda_{os,PCET}$ was approximated using Eq. S2, where θ is the angle between the ET and PT vectors.[22] It was determined via analysis of the structure of a constrained optimization (in which the Fe−H–Co distance was kept constant) that θ is between 0 and 45°, a range which corresponds to an insignificant variation (less than 0.2 kcal mol^{-1}) in $\lambda_{os,PCET}$.

$$\lambda_{os,PCET} = \lambda_{os,PT} + \lambda_{os,ET} - (\lambda_{os,PT} * \lambda_{os,ET})\cos(\theta) \qquad \text{(Eq. S2)}$$

Relative rates for a bimolecular PT/ET vs PCET (k_{bi}) pathway for reaction shown in Table S8, Equation 6 were determined via the method outline by the group of Hammes-Schiffer in which the bimolecular rate constant for PT, ET or PCET is approximated by Eq. S3.

$$k_{bi} = K_A * k_{uni} \quad \text{(Eq. S3)}$$

K_A represents the pre-arrangement equilibrium constant and k_{uni} represents the unimolecular rate constant for PCET or ET.[25] Along an PT/ET pathway, the barriers calculated suggest that $k^{PT} > k^{ET}$. In approximating k_{uni} for PCET and ET, we made extensive use of the webPCET portal.[26] The electronic coupling for PCET and ET was assumed to be equal. In order to approximate a lower bound for k^{PCET}/k^{ET}, the pre-arrangement equilibrium (K_A) was also assumed to be equal for PCET and ET. We believe this represents a lower bound as the approximation for K_A does not include any hydrogen bonding interactions for a PCET pathway.

Method B. Optimization of a 1st Order Saddle Point. PT barriers for the protonation of Cp^*_2Co were also found by optimization of a 1st order saddle point. That the optimized structure represented a 1st order saddle point was confirmed with a frequency calculation, which showed only one imaginary frequency.

Table S8. Overview of Parameters Used to Calculate Kinetic Barriers

1. $[^{2,6\text{-Cl}}PhNH_3][OTf] + Cp^*_2Co \rightarrow Cp^*Co(exo\text{-}\eta^4\text{-}C_5Me_5H)\text{-}OTf + {}^{2,6\text{-Cl}}PhNH_2$
2. $[^{2,6\text{-Me}}PhNH_3][OTf] + Cp^*_2Co \rightarrow Cp^*Co(exo\text{-}\eta^4\text{-}C_5Me_5H)\text{-}OTf + {}^{2,6\text{-Me}}PhNH_2$
3. $[^{4\text{-OMe}}PhNH_3][OTf] + Cp^*_2Co \rightarrow Cp^*Co(exo\text{-}\eta^4\text{-}C_5Me_5H)\text{-}OTf + {}^{4\text{-OMe}}PhNH_2$
4. $P_3{}^BFeNNH + [Cp^*Co(exo\text{-}\eta^4\text{-}C_5Me_5H)][OTf] \rightarrow [P_3{}^BFeNNH_2][OTf] + Cp^*_2Co$
5. $[P_3{}^BFeNNH_2][OTf] + Cp^*_2Co \rightarrow P_3{}^BFeNNH_2 + [Cp_2{}^*Co][OTf]$
6. $P_3{}^BFeNNH + [Cp^*Co(exo\text{-}\eta^4\text{-}C_5Me_5H)][OTf] \rightarrow P_3{}^BFeNNH_2 + [Cp^*_2Co][OTf]$

Reaction	λ_{is}	λ_{os}	Barrier $\{k_{rel}\}$	Method
1	N/A	N/A	1.3 kcal mol^{-1}	A
1	7.5 kcal mol^{-1}	6.3 kcal mol^{-1}	1.3 kcal mol^{-1}	B
2	N/A	N/A	3.8 kcal mol^{-1}	A
2	7.5 kcal mol^{-1}	6.3 kcal mol^{-1}	3.6 kcal mol^{-1}	B
3	N/A	N/A	4.5 kcal mol^{-1}	A
3	7.5 kcal mol^{-1}	6.3 kcal mol^{-1}	4.8 kcal mol^{-1}	B
4	8.9 kcal mol^{-1}	6.3 kcal mol^{-1}	1.5 kcal mol^{-1}	A
5	8.9 kcal mol^{-1}	25.0 kcal mol^{-1}	4.1 kcal mol^{-1} $\{k_{rel} \equiv 1\}$	A[a]
6	13.7 kcal mol^{-1}	0-10 kcal mol^{-1}	0.2 – 0.6 kcal mol^{-1} {2000 – 4500}	A

[a] The barrier for $[P_3{}^BFeNNH_2][OTf]$ reduction was calculated assuming that rate-determining reduction to $[P_3{}^BFeNNH_2][OTf]^-$ precedes OTf^- release.

S10.3. BDFE Calculations

Bond dissociation free energies (BDFE) of X–H bonds were calculated in the gas-phase using a series of known reference compounds.[27] The free-energy difference between the H-atom donor/acceptor pair was calculated based on the thermochemical information provided by

frequency calculations after structure optimizations using the procedure described in the general computational section. A linear plot of ΔG vs $BDFE_{lit}$ was generated to form a calibration curve (**Figure S7.**). BDFE predictions were generated by application of the line of best fit to the calculated ΔG of the unknown species.

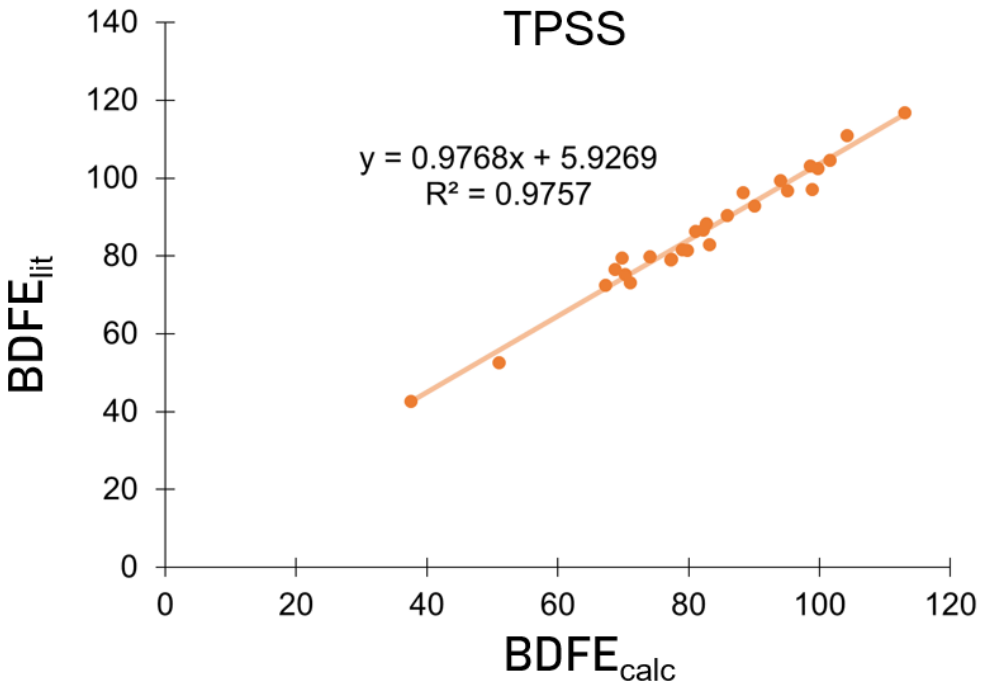

Figure S7. $BDFE_{calc}$ and $BDFE_{lit}$ plotted for species of known $BDFE_{E-H}$. Line of best fit is shown.

Table S9. Data used to generate the plot and line of best fit shown in Figure S5.

Species	ΔG (E-H) (kcal mol^{-1})	ΔG ($E^{\bullet}$) (kcal mol^{-1})	ΔG_{calc} (kcal mol^{-1})	$BDFE_{E-H}$ (kcal $mol^{-1)}$
HOOH	−151.4	−150.8	69.8	79.7
MeOH	−115.6	−115.0	88.3	96.4
EtOOH	−230.0	−229.4	68.7	76.6
H_2O	−76.4	−75.7	104.2	111.0
NH_3	−56.5	−55.8	94.0	99.4
Me_3CH	−158.3	−157.6	82.7	88.3

PhOH	−307.2	−306.6	74.0	79.8
Et_2NH	−213.6	−212.9	81.0	86.4
NH_2NH_2	−111.8	−111.1	67.3	72.6
OH^-	−75.7	−75.0	98.6	103.1
PhSH	−630.2	−629.5	70.3	75.3
NH_4^+	−56.8	−56.1	113.0	116.9
Me_2CH_2	−119.0	−118.4	85.9	90.4
HC(O)OOH	−264.7	−264.1	82.2	86.8
OOH	−150.8	−150.2	37.5	42.7
C_6H_6	−232.1	−231.4	101.6	104.7
C_2H_4	−78.5	−77.8	99.7	102.5
C_2H_6	−79.7	−79.1	90.0	92.9
$PhCH_3$	−271.3	−270.7	79.0	81.6
CH_4	−40.5	−39.8	95.1	96.8
CpH	−193.9	−193.3	71.0	73.2
EtSH	−477.8	−477.2	77.2	79.1
MeSH	−438.6	−437.9	77.3	79.2
$PhNH_2$	−287.4	−286.7	79.8	81.5
NHNH	−110.6	−110.0	51.0	52.6
H_2S	−399.3	−398.7	83.1	83.0
H_2	−1.2	−0.5	98.8	97.2

S10.4. Calculated Reduction Potentials for Selected $[Ar_nNH_{(4-n)}][OTf]$ and $Ar_nNH_{(3-n)}$

Table S10. Calculated Reduction Potentials of Selected Species

Species	E^o (V vs $Fc^{+/0}$)
$[^{4\text{-OMe}}PhNH_3][OTf]$	−3.8 V
$^{4\text{-OMe}}PhNH_2$	−3.4 V
$[^{2,6\text{-Me}}PhNH_3][OTf]$	−3.8 V
$[^{2,6\text{-Cl}}PhNH_3][OTf]$	−2.4 V
$[^{2,6\text{-Cl}}PhNH_3]^+$	−2.0 V
$[Ph_2NH_2]^+$	< −2.5 V[a]
Ph_2NH	−3.1 V
$[^{per\text{-Cl}}PhNH_3][OTf]$	−2.0 V
Cp^*_2Co	−2.2 V

[a] Potential for the formation of $Ph_2NH^\bullet + H^\bullet$ is reported. No 'reversible' minima was found.

S10.5 Discussion of the Anomalous Behavior of $[^{per\text{-Cl}}PhNH_3][OTf]$

Determining the reduction potential of the acids using electrochemical techniques is challenging due to the significant, electrode catalyzed HER observed upon scanning anodically (see Figure S8). However, as expected due to the lower pK_a of $[^{per\text{-Cl}}PhNH_3][OTf]$ compared to $[Ph_2NH_2][OTf]$ we see an earlier onset of the reduction potential and a higher current density. These processes are likely electrode-mediated and thus do not reflect a pure reduction potential, so to better estimate the outer-sphere reduction potential of the acids employed we have used DFT (Table S10). In many cases, attempts to optimize the one electron reduced species results in a chemical step (*i.e.*, loss of Cl^- or H•) precluding determination of the reversible redox potential for the system. We are, however, able to find (*in silico*) a well-behaved reduction for $[^{per\text{-Cl}}PhNH_3][OTf]$ of −2.0 V. As a comparison, the high efficiency acid, $[^{2,6\text{-Cl}}PhNH_3][OTf]$, has a reduction potential of −2.4 V. This leads us to believe for $[^{per\text{-Cl}}PhNH_3][OTf]$ rather than engaging in an inner-sphere proton transfer with Cp^*_2Co ($E^0_{calc}(Cp^*_2Co^{0/+})$ = −2.18 V) it is likely that an outer sphere electron transfer occurs first. This change in mechanism would explain the increased H_2 yields and the decreased N_2RR efficiency. In contrast, $[^{2,6\text{-Cl}}PhNH_3][OTf]$ should be resistant to reduction and thus able to protonate the metallocene and engage in the mechanism discussed in the main text.

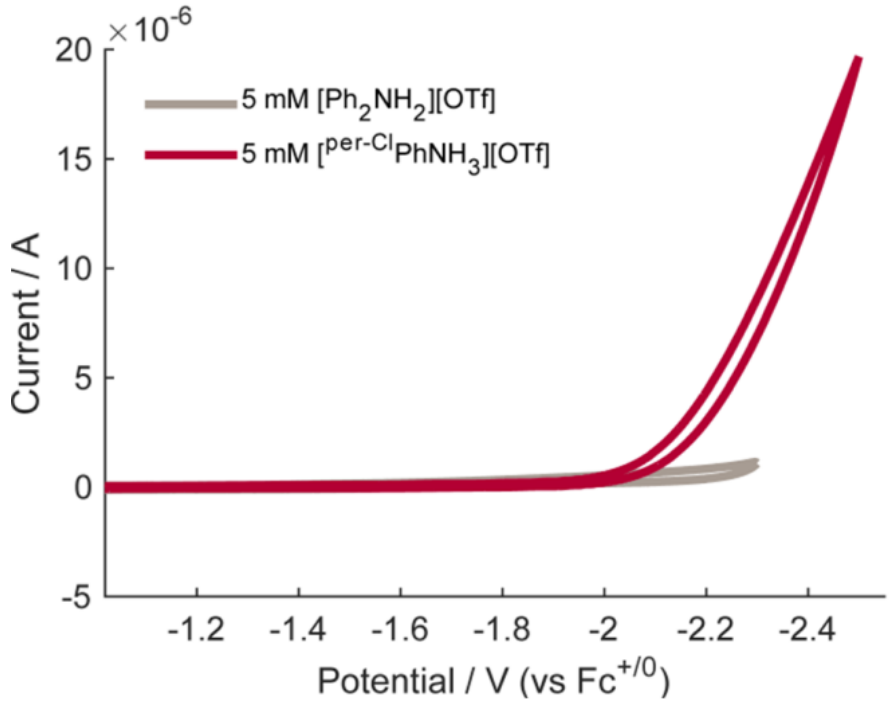

Figure S8. Cyclic voltammograms of 5 mM [Ph_2NH_2][OTf] (gray trace) and 5 mM [$^{per\text{-}Cl}PhNH_3$][OTf] (red trace). All spectra are collected in 0.1 M $NaBAr^F_4$ solution in Et_2O at −35 °C using a glassy carbon working electrode and externally referenced to the $Fc^{+/0}$ couple. Scan rate is 100 mV/s.

S11. X-ray Photoelectron Spectroscopy (XPS) details

The surface composition of the carbon electrode surface after a 15 hour bulk electrolysis in the presence of $[P_3{}^BFe][BAr^F{}_4]$, $[Cp^*{}_2Co][BAr^F{}_4]$, $[Ph_2NH_2][OTf]$ and N_2 was determined via XPS on a Kratos Axis Nova spectrometer with DLD (Kratos Analytical; Manchester, UK). The excitation source for all analysis was monochromatic Al $K\alpha_{1,2}$ ($h\nu$ = 1486.6 eV) operating at 10 mA and 15 kV. The X-ray source was directed at 54° with respect to the sample normal. A base pressure of 1×10^{-9} Torr is maintained in the analytical chamber, which rises to 5×10^{-9} Torr during spectral acquisition. All spectra were acquired using the hybrid lens magnification mode and slot aperture, resulting in an analyzed area of 700 μm × 400 μm. Survey scans were collected using 160 eV pass energy, while narrow region scans used 10 eV; charge compensation via the attached e^--flood source was not necessary in this study.

Subsequent peak fitting and composition analysis was performed using CasaXPS version 2.3.16 (Casa Software Ltd.; Teignmouth, UK). Energy scale correction for the survey and narrow energy regions was accomplished by setting the large component in the C 1s spectrum, corresponding to a C 1s C(=C) transition, to 284.8 eV. All components were fit using a Gaussian 30% Lorentzian convolution function. For quantification, Shirley baselines were employed where there was a noticeable change in CPS before and after the peak in the survey spectrum; otherwise, linear was chosen. Atomic percentages were calculated using the CasaXPS packages for regions and/or components and are reported herein. Calculations were performed using region or component areas normalized to relative sensitivity factors specific to the instrument conditions with deconvolution from the spectrometer transmission function.

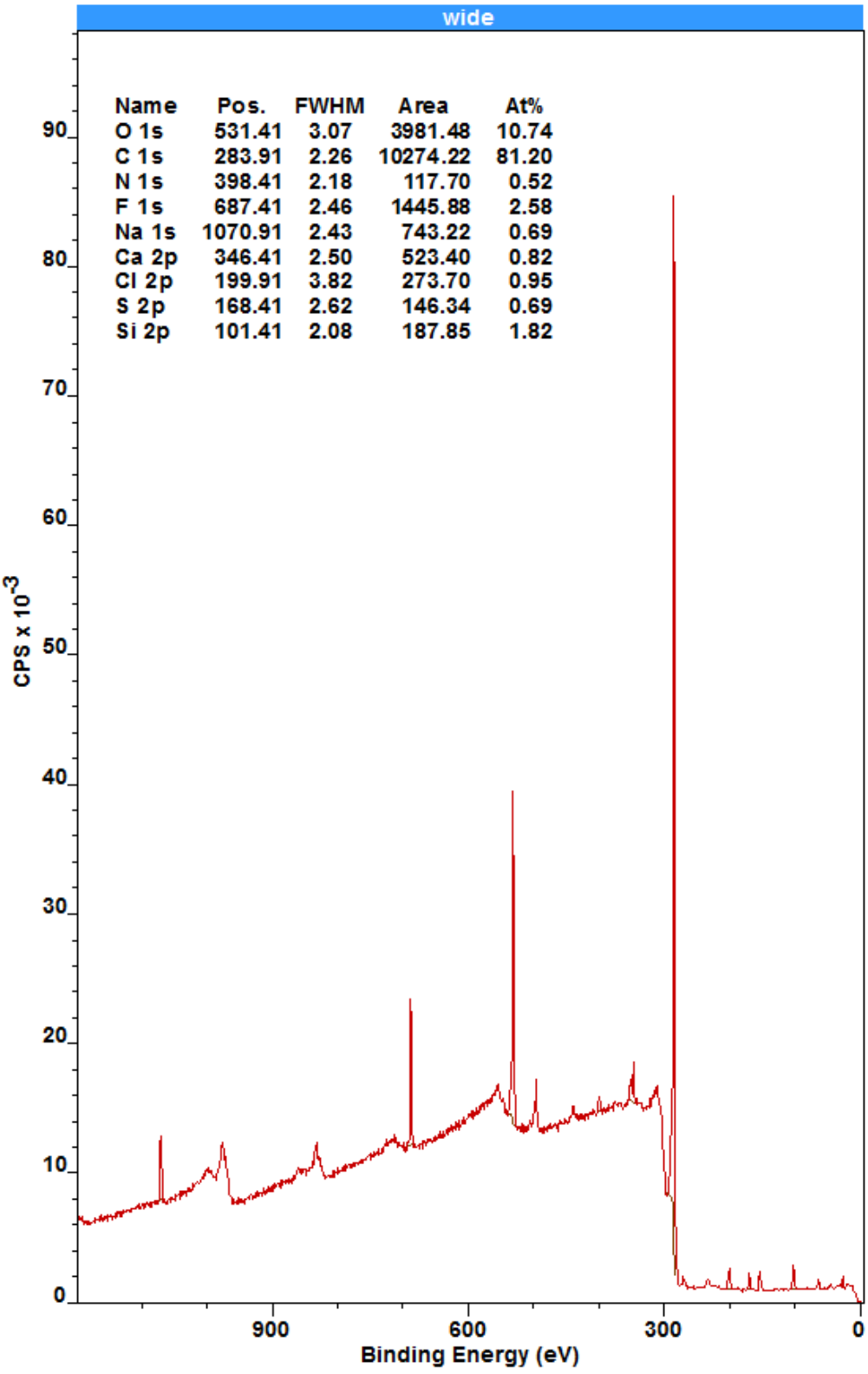
wide
Name Pos. FWHM Area At%
O 1s 531.41 3.07 3981.48 10.74
C 1s 283.91 2.26 10274.22 81.20
N 1s 398.41 2.18 117.70 0.52
F 1s 687.41 2.46 1445.88 2.58
Na 1s 1070.91 2.43 743.22 0.69
Ca 2p 346.41 2.50 523.40 0.82
Cl 2p 199.91 3.82 273.70 0.95
S 2p 168.41 2.62 146.34 0.69
Si 2p 101.41 2.08 187.85 1.82
CPS x 10^-3
90
80
70
60
50
40
30
20
10
0
900
600
300
0
Binding Energy (eV)

Figure S9. XPS survey scan of a section of a glassy carbon plate which <u>was not</u> exposed to the working chamber solution during a 15 hour bulk electrolysis in the presence of $[P_3^BFe][BAr^F_4]$, $[Cp^*_2Co][BAr^F_4]$, $[Ph_2NH_2][OTf]$ and N_2 at −2.1 V (vs $Fc^{+/0}$). XPS and Auger peaks are assigned as labeled in the legend, which also includes atomic percentages calculated from component fits from scans of individual XPS regions. This material represents a baseline of the electrode surface composition resulting from cleaning, polishing, and handling prior to CPE experiments and is provided for comparison to a XPS survey scan of a section of the same glassy carbon plate which was exposed to the working chamber solution during a 15 hour bulk electrolysis in the presence of $[P_3^BFe][BAr^F_4]$, $[Cp^*_2Co][BAr^F_4]$, $[Ph_2NH_2][OTf]$ and N_2 at −2.1 V (vs $Fc^{+/0}$) presented in figure S10.

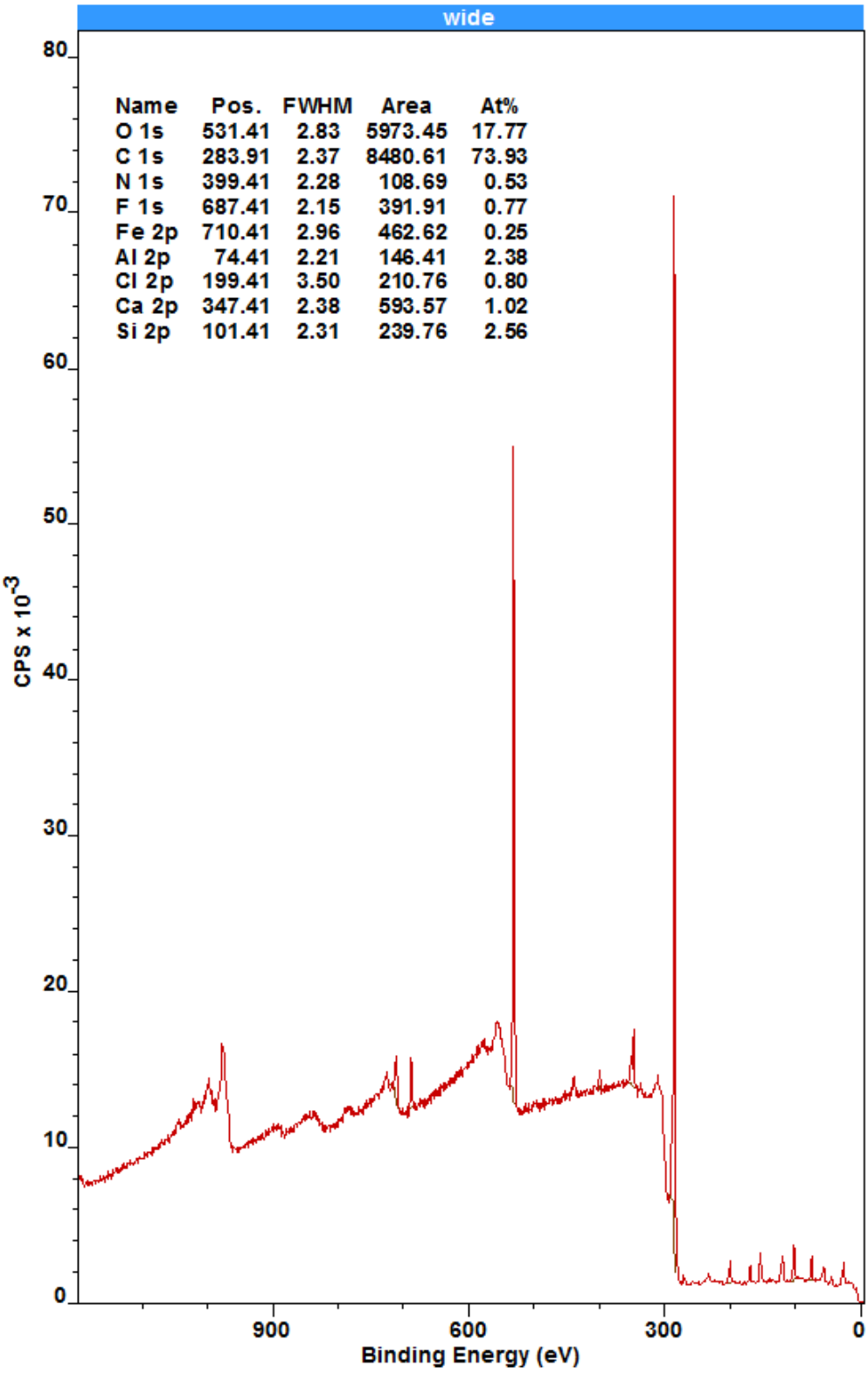
wide
Name Pos. FWHM Area At%
O 1s 531.41 2.83 5973.45 17.77
C 1s 283.91 2.37 8480.61 73.93
N 1s 399.41 2.28 108.69 0.53
F 1s 687.41 2.15 391.91 0.77
Fe 2p 710.41 2.96 462.62 0.25
Al 2p 74.41 2.21 146.41 2.38
Cl 2p 199.41 3.50 210.76 0.80
Ca 2p 347.41 2.38 593.57 1.02
Si 2p 101.41 2.31 239.76 2.56
CPS x 10-3
80
70
60
50
40
30
20
10
0
900
600
300
0
Binding Energy (eV)

Figure S10. XPS survey scan of a section of a glassy carbon plate which was exposed to the working chamber solution during a 15 hour bulk electrolysis in the presence of $[P_3^BFe][BAr^F_4]$, $[Cp^*_2Co][BAr^F_4]$, $[Ph_2NH_2][OTf]$ and N_2 at −2.1 V (vs $Fc^{+/0}$). XPS and Auger peaks are assigned as labeled in the legend, which also includes atomic percentages calculated from component fits from scans of individual XPS regions. This material represents a post-electrolysis state of the electrode surface composition for comparison to a XPS survey scan of a section of the same glassy carbon plate which was exposed to the working chamber solution during a 15 hour bulk electrolysis in the presence of $[P_3^BFe][BAr^F_4]$, $[Cp^*_2Co][BAr^F_4]$, $[Ph_2NH_2][OTf]$ and N_2 at −2.1 V (vs $Fc^{+/0}$) presented in figure S1. Notably this active surface scan reveals a small Fe signal, likely resulting from some degree of decomposition of the $[P_3^BFe][BAr^F_4]$ catalyst over the course of the 15 hour electrolysis; however it is also possible that this small Fe signal is the result of contamination during the handling of the sample. This Fe 2p signal occurs at 710.4 eV, but due to the weak signal intensity it is not possible to confidently assign its oxidation state. Although, the signal does not appear consistent with Fe(0) whose signal is typically around 707 eV;[28] we would also note though that the handling process involves transferring the electrode quickly in air which could result in oxidation of Fe(0) that was present. Also notable is that no new Co signal is observed in the post-electrolysis scan suggesting that $[Cp^*_2Co][BAr^F_4]$ does not decompose to a surface bound Co species in detectable amounts during the electrolysis. Phosphorus was not detectable in this survey scan; however, in a reproduction of this experiment, phosphorus was detected in an XPS scan of an electrode used for electrolysis. In that experiment the signal was too small for quantitation..

S12. pK_a Determination Strategy

Bosch et al. published a procedure for converting a pK_a in THF into the equivalent pK_a in different solvents.[29] Although not all of the pK_a values have been experimentally determined in THF the values obtained from converting from MeCN or H_2O into a THF value is quite accurate. So we have used these converted values in the text. Where available a number measured in THF has been used, if not the MeCN derived value is used. If neither is available then the H_2O derived value is used.

Solvent conversion equations:

$$pK_a(THF) = 0.78 \times pK_a(MeCN) - 0.52$$

$$pK_a(THF) = 1.19 \times pK_a(H_2O) + 2.13$$

Acid	pK_a in MeCN	pK_a in H_2O	Converted pK_a [a]	Experimental pK_a in THF

[$^{4\text{-OMe}}$PhNH$_3$][OTf]	11.86[30]	5.29[32]	8.8 (8.4)	8.8[29]
[PhNH$_3$][OTf]	10.62[30]	4.58[32]	7.8 (7.6)	8.0[29]
[$^{2,6\text{-Me}}$PhNH$_3$][OTf]	--	3.89[32]	-- (6.8)	
[$^{2\text{-Cl}}$PhNH$_3$][OTf]	7.86[30]	2.64[32]	5.6 (5.3)	6.0[29]
[$^{2,5\text{-Cl}}$PhNH$_3$][OTf]	6.21[31]	1.53[30]	4.3 (4.0)	4.5[29]
[$^{2,6\text{-Cl}}$PhNH$_3$][OTf]	5.06[30]	0.42[33]	3.4 (2.6)	
[$^{2,4,6\text{-Cl}}$PhNH$_3$][OTf]	--	−0.03[33]	-- (2.1)	
[$^{\text{per-Cl}}$PhNH$_3$][OTf]	2.35[31]	--	1.3 (--)	
collidinium triflate	14.98[30]	--	11.2 (--)	
benzylammonium triflate	--	9.34[34]	-- (13.2)	

[a]First is listed the value converted from THF and then in parentheses is the value converted from H_2O.

S13. References

[1] Robbins, J. L.; Edelstein, N.; Spencer, B.; Smart, J. C. *J. Am. Chem. Soc.* **1982**, *104*, 1882.
[2] Anderson, J. S.; Moret, M.-E.; Peters, J. C. *J. Am. Chem. Soc.* **2013**, *135*, 534.
[3] Moret, M.-E.; Peters, J. C. *J. Am. Chem. Soc.* **2011**, *133*, 18118.
[4] Del Castillo, T. J.; Thompson, N. B.; Peters, J. C. *J. Am. Chem. Soc.* **2016**, *138*, 5341.
[5] Melzer, M. M.; Mossin, S.; Dai, X.; Bartell, A. M.; Kapoor, P.; Meyer, K.; Warren, T. H. A *Angew. Chem. Int. Ed.* **2010**, *49*, 904.
[6] Vicente, J.; Chicote, M.-T.; Guerrero, R.; Jones, P. G. *J. Chem. Soc., Dalton Trans.* **1995**, *8*, 1251.
[7] Grimme, S.; Antony, J.; Ehrlich, S.; Krieg, H. *J. Chem. Phys.* **2010**, *132*, 154104.
[8] Tao, J.; Perdew, J. P.; Staroverov, V. N.; Scuseria, G. E. *Phys. Rev. Lett.* **2003**, *91*, 146401.
[9] Weigend, F.; Ahlrichs, R. *Phys. Chem. Chem. Phys.* **2005**, *7*, 3297.
[10] Towns, J.; Cockerill, T.; Dahan M.; Foster, I.; Gaither, K.; Grimshaw, A.; Hazlewood, V.; Lathrop, S.; Lifka, D.; Peterson, G. D.; Roskies, R.; Scott, J. R.; Wilkins-Diehr, N. *Comput. Sci. Eng.* **2014**, *16*,62-74.
[11] Valiev, M.; Bylaska, E. J.; Govind, N.; Kowalski, K.; Straatsma, T. P.; Van Dam, H. J. J.; Wang, D.; Nieplocha, J.; Apra, E.; Windus, T. L.; de Jong, W. A. *Comput. Phys. Commun.* **2010**, *181*, 1477.
[12] Neese, F. *Wiley Interdiscip. Rev.: Comput. Mol. Sci.* **2012**, *2*, 73.
[13] Klamt, A.; Schüürmann, G. *J. Chem. Soc. Perkin Trans. 2.* **1993**, *2*, 799.
[14] Marten, B.; Kim, K.; Cortis, C.; Friesner, R. A.; Murphy, R. B.; Ringnalda, M. N.; Sitkoff, D.; Honig, B. *J. Phys. Chem.* **1996**, *100*, 11775.
[15] Ribeiro, R. F.; Marenich, A. V.; Cramer, C. J.; Truhlar, D. G. *J. Phys. Chem. B* **2011**, *115*,

14556.
[16] Wang, T.; Brudvig, G.; Batista, V. S. *J. Chem. Theory Comput.* **2010**, *6*, 755.
[17] Hamashima, Y.; Somei, H.; Shimura, Y.; Tamura, T.; Sodeoka, M. *Org. Lett.* **2004**, *6*, 1861.
[18] Anderson, L. L.; Arnold, J.; Bergman, R. G. *J. Amer. Chem. Soc.* **2005**, *127*, 14542.
[19] Anderson, J. S.; Cutsail, G. E., III; Rittle, J.; Connor, B. A.; Gunderson, W. A.; Zhang, L.; Hoffman, B. M.; Peters, J. C *J. Am. Chem. Soc.* **2015,** *137*, 7803.
[20] Stoll, S.; Schweiger, A. *J. Magn. Reson.* **2006**, *178*, 42.
[21] Marcus, R. A. I. *J. Chem. Phys.* **1956**, *24*, 966.
[22] Iordanova, N.; Decornez, H.; Hammes-Schiffer, S. *J. Am. Chem. Soc.* **2001**, *123*, 3723.
[23] Koper, M. T. M. *Chem. Sci.* **2013**, *4*, 2710.
[24] Onsager, L. *J. Am. Chem. Soc.* **1936**, *58*, 1486.
[25] Thoss, M.; Evers, F. *J. Chem. Phys.* **2018**, *148*, 030901.
[26] (a) *web*PCET Application Server, University of Illinois at Urbana-Champaign, http://webpcet.scs.uiuc.edu (2009) (b) Hammes-Schiffer, S.; Soudackov, A. V. *J. Phys. Chem. B* **2008**, *112*, 14108-14123.
[27] Warren, J. J.; Tronic, T. A.; Mayer, J. M. *Chem. Rev.* **2010**, *110*, 6961.
[28] Biesinger, M. C.; Payne, B. P.; Grosvenor, A. P.; Lau, L. W. M.; Gerson, A. R.; Smart, R. S. C. *Appl. Surf. Sci.* **2011**, *257*, 2717.
[29] Garrido, M. Rosés, C. Ràfols, E. Bosch *J. Soln. Chem.* **2008**, *37*, 689.
[30] Kaljurand, I.; Kütt, A.; Sooväli, L.; Rodima, T.; Mäemets, V.; Leito, I.; Koppel, I. A. *J. Org. Chem.* **2005**, *70*, 1019.
[31] Haav, K.; Saame, J.; Kütt, A.; Leito, I. *Eur. J. Org. Chem.* **2012**, 2167.
[32] Pankratov, A. N.; Uchaeva, I. M.; Doronin, S. Y.; Chernova, R. K. *J. Struct. Chem.* **2001**, *42*, 739.
[33] Liao, K.; Pack, B. W.; Toltl, N. P. *J. Pharm. Biomed. Anal.* **2007**, *44*, 118.
[34] Hall, H. K. *J. Am. Chem. Soc.* **1957**, *79*, 5441.